Journal of Alloys and Compounds 774 (2019) 1216–1222

Contents lists available at ScienceDirect

Journal of Alloys and Compounds

journal homepage: http://www.elsevier.com/locate/jalcom

Compressive deformation of MoAlB up to 1100 °C

Yexiao Chen [a], Sankalp Kota [b], Michel W. Barsoum [b, **], Miladin Radovic [a, *]

[a] Department of Materials Science and Engineering, Texas A&M University, College Station, TX 77843, USA
[b] Department of Materials Science and Engineering, Drexel University, Philadelphia, PA 19104, USA

ARTICLE INFO

Article history:
Received 11 April 2018
Received in revised form
10 September 2018
Accepted 11 September 2018
Available online 27 September 2018

Keywords:
Brittle-to-plastic transition
Kinking
Compression
Microcracking

ABSTRACT

Quasi-static and cyclic compression tests at room and high temperatures were conducted on MoAlB, which has an atomically laminated structure that consists of a Mo-B sublattice interleaved by double layers of pure Al. The results show that MoAlB goes through a brittle-to-plastic transition (BPT) at around 800 °C. Below the BPT temperature, MoAlB behaves as a linear-elastic solid and fails in a brittle manner at stresses exceeding 2 GPa despite the fact that the grain size was 6 ± 1 μm. While post-testing microstructural observation showed only a few bends and kinks of individual grains, extensive microcracking was observed. Above the BPT temperature, the deformation was non-linear elastic with open stress-strain hysteresis loops and small irrecoverable strains after each loading-unloading cycle. This behavior was attributed predominantly to micocracks that appear to be constrained mostly within a shear band and coalesce into larger cracks.

1. Introduction

Transition metal borides (TMB) are an appealing class of refractory materials because of their high melting points, high hardness, good corrosion resistance in many environments, and good electrical/thermal conductivities. This set of properties, among others, make them useful for high-temperature structural applications, wear-resistant coatings, diffusion barriers, high-temperature electrodes, solar absorbers, catalysts, etc. [1–6]. However, their utilization in many of those applications is limited because of their inherent mechanical brittleness, poor oxidation and thermal shock resistance, and relatively high cost [7].

First synthesized in the 1950s by Jeitschko [8], MoAlB crystallizes in the orthorhombic space group *Cmcm* with a structure that consists of a Mo-B sublattice interleaved with double layers of pure Al. In this regard, MoAlB has an atomically laminated structure analogous to those of the ternary transition metal carbides and nitrides, commonly referred to as MAX phases [9]. Recently, MoAlB was synthesized as a dense, predominantly single-phase ceramic and found to be quite oxidation resistant due to the formation of a well-adhered, and protective, Al_2O_3 scale up to 1350 °C in ambient air [10–12], which shows that MoAlB has the potential to overcome some of the limitations faced by TMBs in high-temperature oxidizing environments.

Using resonant ultrasound spectroscopy (RUS), the room temperature (RT) Young's and shear moduli were measured to be 373 and 151 GPa, respectively. The corresponding values at 1200 °C were 320 GPa and 130 GPa, respectively, which are ~86% of the RT values [10]. At 10.6 GPa, the Vickers hardness was considerably lower than those of MoB, MoB_2 and most other binary TMBs [13,14], but significantly higher than the typical MAX phase. However, as in MAX phases, the indentation marks in MoAlB lack the large, dominant cracks emanating from the corners that are commonly observed in brittle ceramics. The latter suggests that this material could have decent damage tolerance. In our previous work, we also reported ultimate compressive stresses (UCS) between 1.4 and 1.9 GPa depending on the orientation of the loading axis relative to the hot pressing direction [12]. In MoAlB fabricated by hot-pressing pre-reacted MoAlB powders, Xu et al. found similar compressive strengths (1.3–1.6 GPa) and hardness values (~9.3 GPa under a 30 N load). In addition, they reported a fracture toughness value of 4.3 MPa $m^{1/2}$ and flexural strengths of 456 MPa at RT [15].

While these properties bode well for the potential use of MoAlB at high temperatures in ambient air, deeper understanding of its mechanical properties and of the operative deformation and failure mechanisms at both room and elevated temperatures is needed. The atomically laminated structure and large *b*/*a* and *b*/*c* ratios (i.e. ratio of lattice constant parallel to perpendicular to the stacking *b*

* Corresponding author.
** Corresponding author.
E-mail addresses: barsoumw@drexel.edu (M.W. Barsoum), mradovic@tamu.edu (M. Radovic).

https://doi.org/10.1016/j.jallcom.2018.09.124
0925-8388/

axis), are features that MoAlB share with their damage tolerant MAX cousins, that can deform *via* intra-grain bending, kinking and delamination [16–18]. Most recently, deformation of MAX phases by ripplocation formation was also proposed in the literature [19,20]. Based on the structural similarities, we postulated that the same micro-mechanisms could also play a major role in the deformation of MoAlB. For example, the nonlinear elastic behavior, first reported in Ti_3SiC_2 [21] and later in many other MAX phases [22–30], was anticipated at both room and higher temperatures.

To test this hypothesis and gain a general understanding of the mechanical properties over a wide temperature range, we quasi-statically and cyclically compressed MoAlB polycrystalline samples up to 1100 °C in ambient air. The microstructural evolution, as a function of loading, was investigated using a scanning electron microscopy, SEM, to elucidate the dominant deformation and failure micromechanisms.

2. Experimental details

A stoichiometric MoB (MoB with Mo:B atomic ratio 1:1, Alfa Aesar, 99%, <38 μm) and Al powders were mixed in a 1.0:1.25 molar ratio in a polyethylene jar, and ball milled with ZrO_2 balls for 24 h. The powder mixtures were poured into a boron nitride-coated graphite die and pre-compacted at 30 MPa. The die was placed in a hot press (HP) and heated under mechanical vacuum (<15 Pa) at a rate of 500 °C/h to 1200 °C and loaded to 25 MPa. The temperature and pressure were held for 5 h before cooling the HP naturally to RT. The bonded graphite from the as-sintered sample was ground off for sample characterization.

The phase composition of the sample was inspected using X-ray diffraction (XRD, Rigaku SmartLab) with Cu Kα radiation between 10 and 80° 2θ using a step size of 0.04° and dwell time of 0.9 s. XRD results, in Fig. 1a, show that as-processed samples contained Al_8Mo_3 impurities. Those results were confirmed using scanning electron microscopy (SEM, Zeiss Supra 50VP), as shown by a representative backscattered electron micrographs in Fig. 1b, and energy dispersive X-ray spectroscopy (EDS, Oxford Instruments). Backscattered electron SEM micrographs (Fig. 1b) and EDS show that Al-rich Al-Mo phases, with Al:Mo ratios similar to Al_8Mo_3, and Al_2O_3 impurities were present. Image contrast analysis on 6 regions, of ~225 × 175 μm^2 each, showed that ~7 vol% and 2 vol% of the two impurities were present, respectively, which is consistent with our previous work [10–12]. Porosity of the samples was determined to be 0.4 ± 0.10% by Archimedes method that is described in more details elsewhere [23,28,29]. A drop of a 2:1:2 part solution, by volume, of hydrofluoric acid (48–51 wt%, Acros Organics), nitric acid (68%, Alfa Aesar, Ward Hill, MA) and water was placed on the sample for 5 s to etch the surface for grain size analysis. A grain size of 6 ± 1 μm was calculated from representative etched SEM micrographs, (Fig. 1c), using the line intersect method with a 2D-to-3D correction factor of 1.2. Note that larger grains with lengths up to 30 μm were occasionally found.

Two kinds of cylindrical samples – smaller ones 4 mm in diameter and 8 mm long and larger ones 8 mm in diameter and 17 mm long were machined by wire electro-discharge machining (Wire-EDM). Dimensions of the small cylinders were selected not to exceed the load limits of the SiC pushrods used for high-temperature testing at the ultimate compressive strength (UCS) of the specimens, while the large cylinders were designed to allow for the attachment of a high-accuracy, high-temperature extensometer.

The smaller samples were quasi-statically compressed to failure using a servo-hydraulic testing machine (MTS-810, MTS, USA) with SiC pushrods at a constant crosshead displacement rate corresponding to a strain rate of 10^{-4} s^{-1}. Cyclic compression testing was

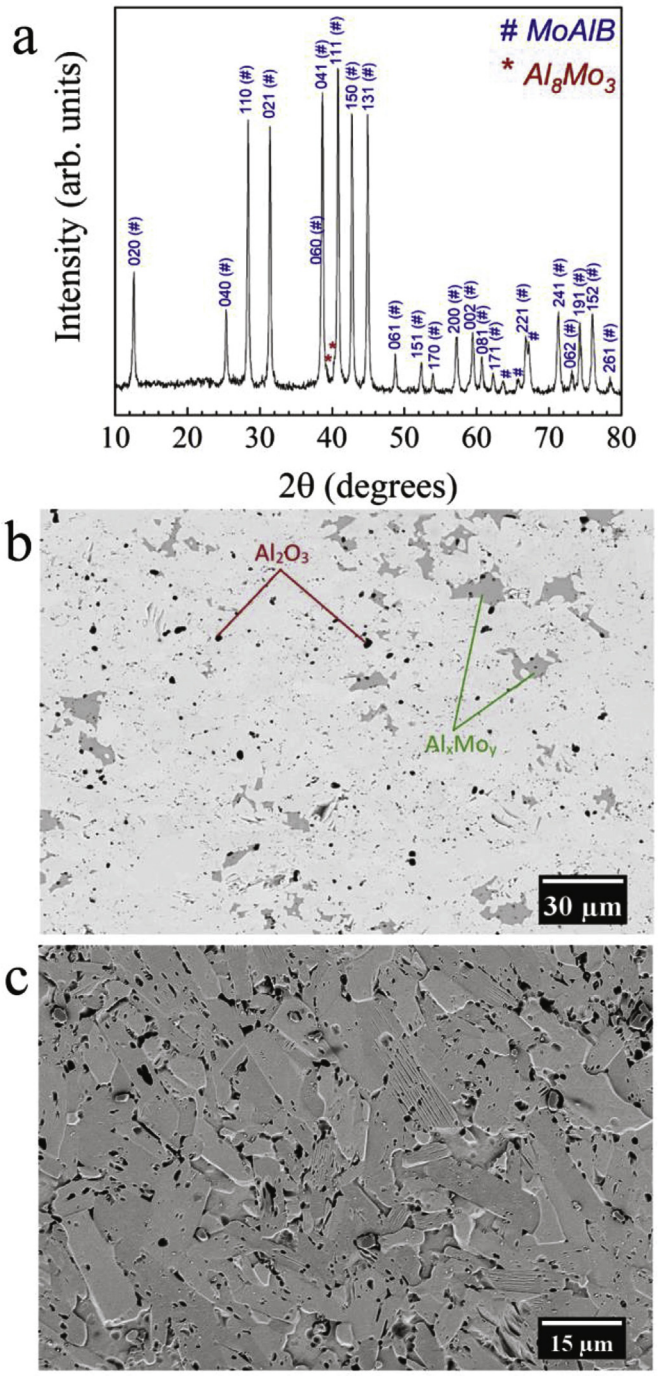

Fig. 1. (a) XRD pattern and, (b) electron-backscatter SEM image of as-processed MoAlB sample before etching and, (c) after etching.

carried out on the larger samples at a frequency of 0.5 Hz, at two stress amplitudes namely 250 MPa and 650 MPa, using the same testing machine. However, in the latter case an axial extensometer (632.59, MTS, USA) attached directly to the samples was used to measure the strains. A preload stress of 55 MPa was applied before each test to ensure good sample alignment and firm contact between sample and pushrods. Typically, samples were loaded to the amplitude stress and unloaded back to the preload stress, for 10 cycles, while monitoring force and strain.

After compression testing, select samples were cut down the

middle along the compression loading direction. The exposed cross-sections were mechanically polished using sand paper and polished with 9 to 1 μm diamond suspensions. For the final polishing step a 0.05 μm colloidal silica solution was used. After polishing the samples were imaged using SEM Quanta 600 FEG (FEI, Oregon, USA) scanning electron microscope.

3. Results

3.1. Temperature dependence of ultimate compressive strength (UCS)

Fig. 2 shows selected, but typical, engineering stress vs. relative crosshead displacement curves and calculated UCS of MoAlB at different temperatures. Note that engineering stress was determined as load divided by initial cross-section area of the sample, while relative crosshead displacement was calculated as crosshead displacement divided by initial height of the sample. At RT, and below 800 °C, the mechanical response is linear elastic until brittle failure. Between 800 and 900 °C, the material starts to show some plastic deformation but still fails in a predominantly brittle manner, i.e. it shatters in a large number of small pieces. Above 1000 °C, extensive plastic deformation is observed. These results suggest the presence of a brittle to plastic (BPT) transition. The reason it is referred to as a BPT and not the more common brittle-to-ductile transition is to emphasize that the transition is not a result of the activation of additional slip systems. Here (see below), like in the MAX phases, the transition is typically accompanied by distributed damage in the form of cracks and delaminations [31]. Just below the BPT temperature, between 600 and 800 °C, the UCS slightly increases with increasing temperature. The significant drop in UCS above 800 °C (Fig. 2b) together with the increases in strain to failure, is evidence that MoAlB goes through a BPT similar to that observed for the MAX phases [17,32,33].

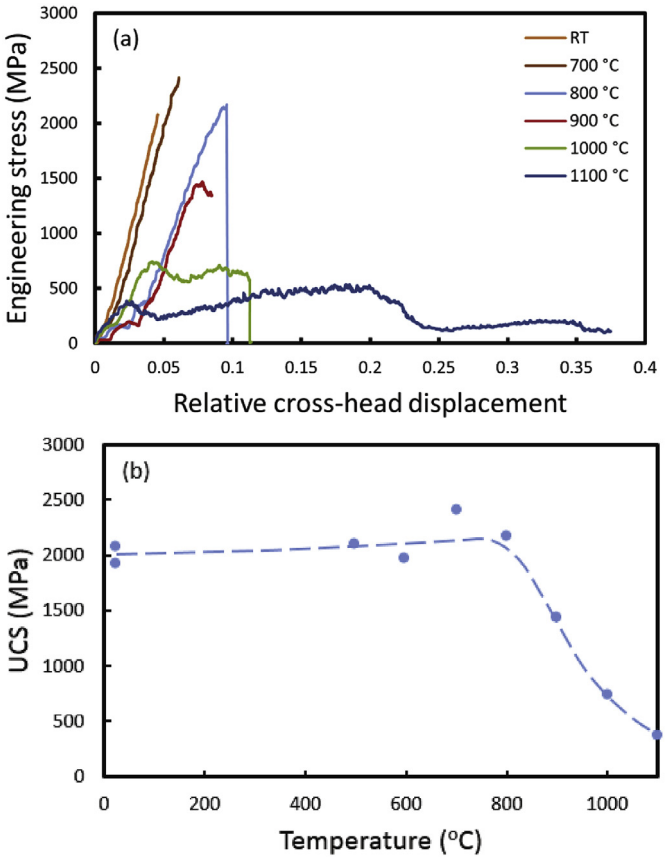

Fig. 2. (a) Selected engineering stress vs. relative cross-head displacement curves at RT, around BPT and above the BPT temperature; (b) Effect of temperature on UCS.

3.2. Quasi-static compression

Select but typical engineering stress-strain curves obtained using the larger samples (8 mm dia. and 17 mm long) are shown in Fig. 3, for samples tested at RT and 1100 °C. Note here that the maximum applied engineering stress was limited to 1.5 GPa which is the load bearing capacity of our SiC pushrods. In other words, the sample tested at RT (Fig. 3) did not fail at 1.5 GPa, and its stress-strain curve was linear-elastic up to that stress.

At 1100 °C, the response was more complicated. The stress-strain curves show that the material initially goes through a linear-elastic regime, after which a transient "hardening" region can be observed (lower curve in Fig. 3). Subsequently, a distinct softening regime is reached, followed by another hardening region where the test is interrupted at 9% strain (the limit of our extensometer). In sharp contrast to most MAX phases, no hysteresis was observed, at RT. However, above the BPT temperature the overall stress-strain behavior is quite similar to that observed in the MAX phases in which strains to failure can exceed 15% in compression at 1100 °C [34,35] and 20% in tension at 1200 °C [33].

3.3. Cyclic compression

The response of MoAlB at RT, 700, 800, 900 and 1000 °C to cyclic loading up to stresses of 250 MPa and 650 MPa using a frequency of 0.5 Hz is shown in Fig. 4. The following points are salient for samples cyclically loaded to 650 MPa: (i) the slope of the initial linear part is consistent with E values determined by RUS indicated by dashed red lines in Fig. 3 [10]; (ii) at RT and 700 °C, no hysteresis was detectable; (iii) Nonlinear stress-strain behavior and irrecoverable deformation can be observed starting at 800 °C. All hysteretic stress-strain loops above 800 °C, are not fully reversible, as indicated by the colored loops of successive cycles at 1000 °C and 650 MPa where 1st, 5th and 10th cycle are highlighted in blue, orange and red, respectively. Said otherwise, some irrecoverable strain is recorded after each loading cycle. The same is true for samples cycled at 250 MPa (bottom panels in Fig. 4); and, (iv) the

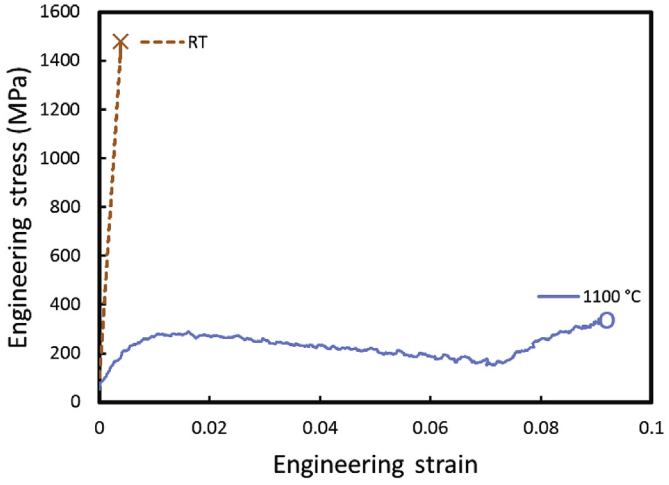

Fig. 3. Typical engineering stress-strain curves obtained in quasi-static compression at RT and 1100 °C. The RT temperature sample did not fail; the test was interrupted to protect the SiC platens.

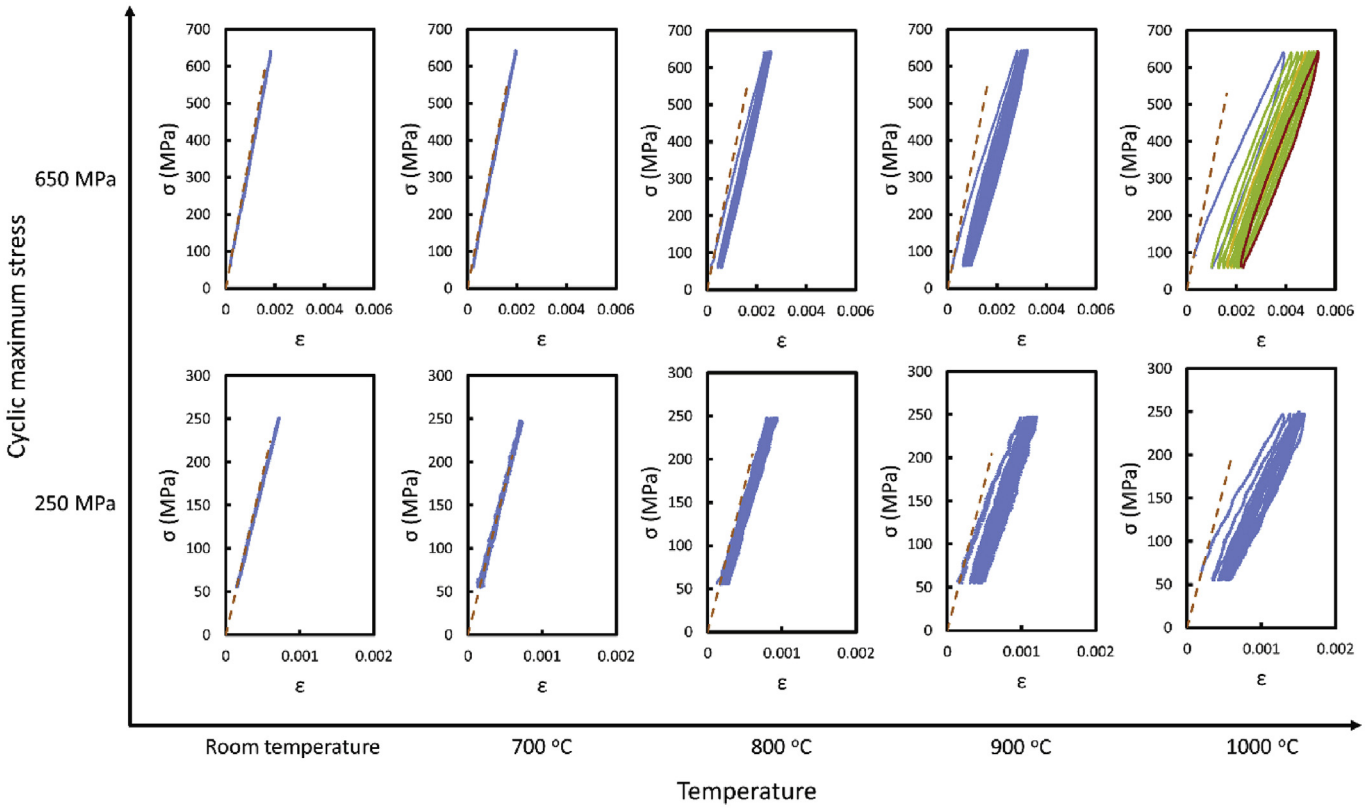

Fig. 4. Engineering stress-strain behavior of MoAlB cyclically loaded/unloaded for 10 cycles with a frequency of 0.5 Hz up to amplitude stresses of 650 MPa (top row) or 250 MPa (bottom row) at temperatures indicated. The dashed lines are the linear elastic response expected from RUS [10].

amount of irrecoverable strain after unloading decreases with increasing number of loading cycles to 650 MPa, as well as the area of the hysteresis loop (Fig. 5). The latter indicates that mechanical energy dissipated in each loading-unloading cycle decreases with increasing number of cycles. The stress-strain curves obtained by loading up to 250 MPa (bottom row of panels in Fig. 4) are qualitatively the same as those obtained at 650 MPa, but with smaller irrecoverable strains and smaller hysteresis loop areas, at and above 800 °C.

The observed stress-strain response of MoAlB below 800 °C is quite different than that of the MAX phases since the latter show reproducible closed hysteresis loops even below their BPT

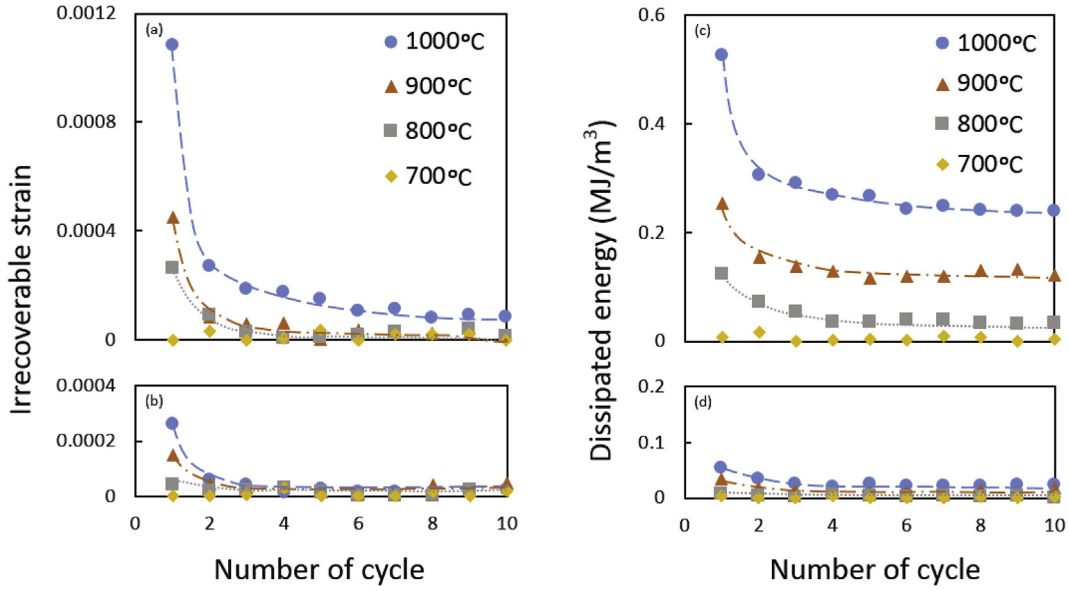

Fig. 5. Irrecoverable strain for samples cyclically loaded to (a) 650 MPa and (b) 250 MPa, and dissipated energy under (c) 650 MPa and (d) 250 MPa, as a function of number of cycles determined from the stress-strain curves shown in Fig. 4.

temperature [17,18]. However, the latter's mechanical responses in cyclic compressive loadings above BPT temperatures are qualitatively similar, with MoAlB having much higher strength at equivalent temperatures. The large irrecoverable strain after the first loading-unloading cycle, that decreases with each subsequent loading, can be observed in both materials, as well as the decreasing size of the hysteresis loop (i.e. energy dissipated per each loading cycle) with number of loading cycles, as is summarized in Fig. 5.

3.4. Microstructural characterization of compressed samples

Fig. 6 shows select, but typical, cross-sectional SEM micrographs of as-sintered MoAlB sample before cyclic compression, (Fig. 6a), after 10 cycles of cyclic compression loading to 650 MPa at 700 °C (Fig. 6b) and 900 °C (Fig. 6c), and quasi-static loading to 9% strain at 1100 °C (Figs. 6d–f). In general, the as-sintered sample (Fig. 6a) and those cyclically compressed at temperatures below BPT, such as that loaded at 700 °C in Fig. 6b, are comparable in that they both show the same micro-laminated structure, with visible *trans*-granular delamination along basal planes. After cyclic compression to 650 MPa at 900 °C, bending of individual grains can be observed, as well as transgranular microcracks perpendicular to the basal planes (Fig. 6c). Eventually, the microcracks coalesce into larger cracks at higher temperatures, as illustrated in the case of quasi-statically loaded sample at 1100 °C in Figs. 6d and e. At a higher magnification (Fig. 6f), some delaminations crack that do not extend along the entire grain are observable, suggesting that delamination is concomitant with bending or kinking of individual grains.

No visible damage accumulation except the above mentioned transgranular delaminations in samples loaded in compression was observed below the BPT temperature. However, as illustrated in Fig. 7 for the sample quasi-statically compressed at 1100 °C, intergranular cracking and voids accumulate in the microstructure, most notably within a shear band (denoted by blue lines in Fig. 7) that is oriented approximately 45° relative to the direction of the applied stress. This shear region also contains bent and kinked grains as those shown in Figs. 6d and e. Finally, it is also important to note that macroscopic cracks and voids are only observed in the crack-rich region (shear band).

4. Discussion

The results presented in Figs. 2–4 clearly show that below 800 °C, MoAlB responds to compressive stresses in a linear elastic manner. This is evidenced by the fact that slopes of the stress-strain curves are in excellent agreement with those measured using RUS (shown by dashed red lines in Fig. 4). The failure is brittle, with UCS in the range of 2–2.5 GPa. These values are noteworthy given the grain size (≈5–30 μm, Figs. 1 and 6) of the samples tested, compared to typical fine-grained MAX phases and alumina, Fig. 8 [31,36–38]. This linear elastic response in MoAlB is different than that of most MAX phases, wherein under compression the response at room temperature is hysteretic [17–23,39–42]. It is worth noting, however, that Ti_2SC as a MAX phase wherein the Ti–S bonds are relatively strong and that is harder than most of the other MAX phases, also responds in a linear elastic fashion when loaded in compression at RT [43].

Above the BPT temperature, however, both the MAX phases and MoAlB deform plastically with extensive strains to failure – at the higher temperature ends – in compression (note 9% strain in Fig. 3 is not the failure strain, but rather the strain at which the test was interrupted). Another similarity is the significant drop in UCS with increasing temperature. Above the BPT temperature, especially at 1100 °C, the stress-strain curve in MoAlB exhibits a linear elastic region, followed by a region of apparent "hardening" and then gradual softening (see Fig. 3). In other words, MoAlB starts to creep due to microcracking. The reason for the second apparent hardening at strains exceeding 7% (Fig. 3) is unclear at this time, but could possibly be related to the significant increase in the cross-sectional area (~48%) due to "barreling" of the sample.

Observed differences in macroscopic stress-strain behavior

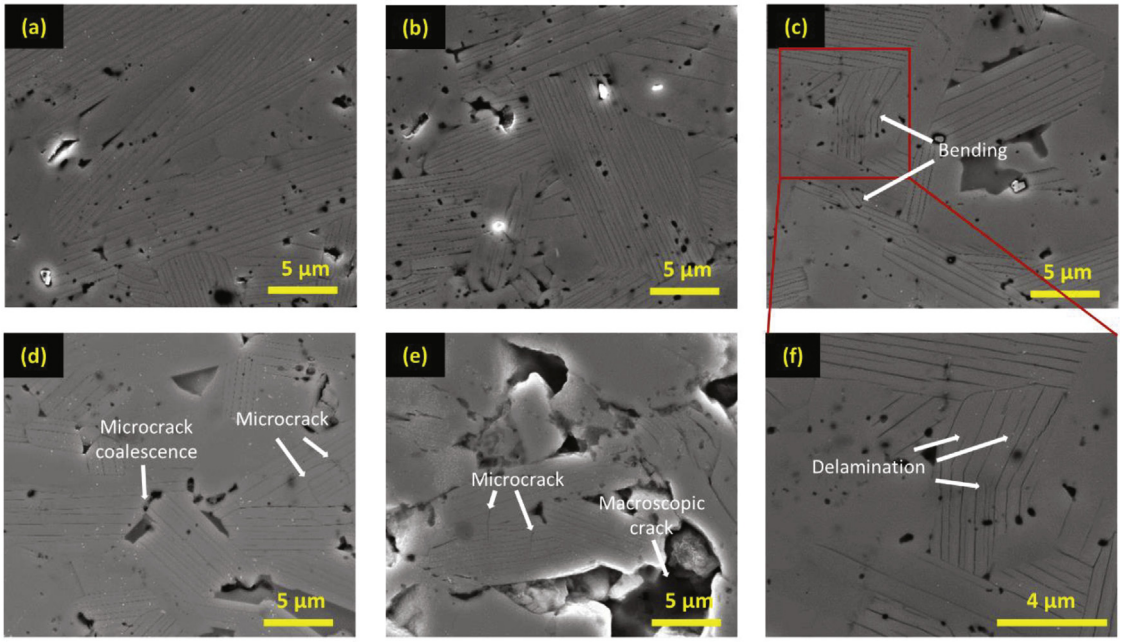

Fig. 6. SEM images of selected MoAlB samples: (a) as-produced; after cyclic compression to 650 MPa at RT, (b) at 700 °C and, (c,f) at 900 °C; after quasi-static compression to a strain of 9% at 1100 °C from, (d) the crack-free region and, (e) crack-rich region (shear band) that are marked in Fig. 7. In all figures, the compressive load was applied in the vertical direction.

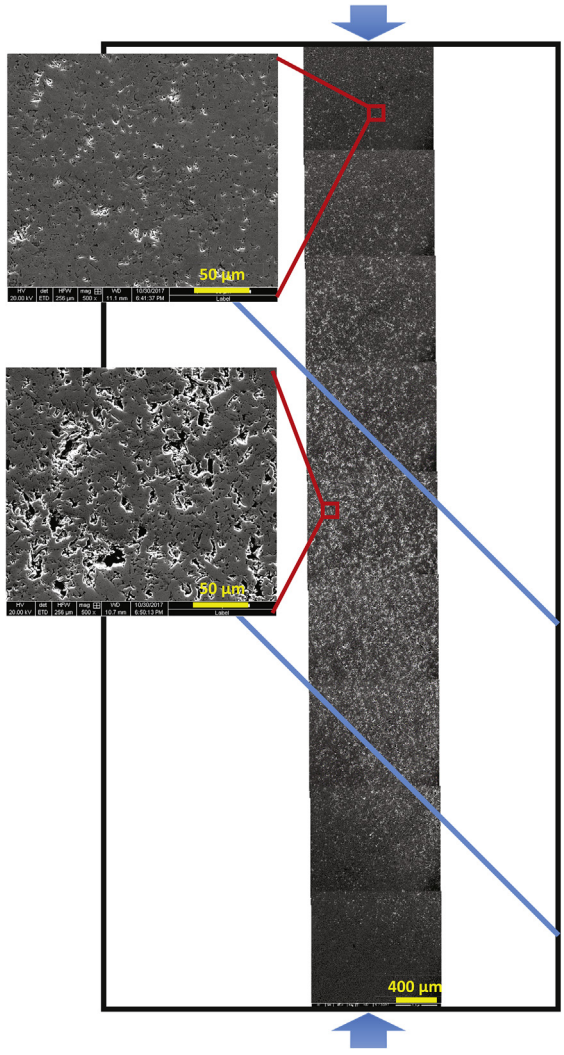

Fig. 7. SEM images taken along the longitudinal axis of the sample's cross-section after quasi-static compression to a strain of 9% at 1100 °C. The black frame outlines the entire sample, while the blue lines highlight a shear band. Arrows denote loading direction. Units of the scale bars are micrometers.

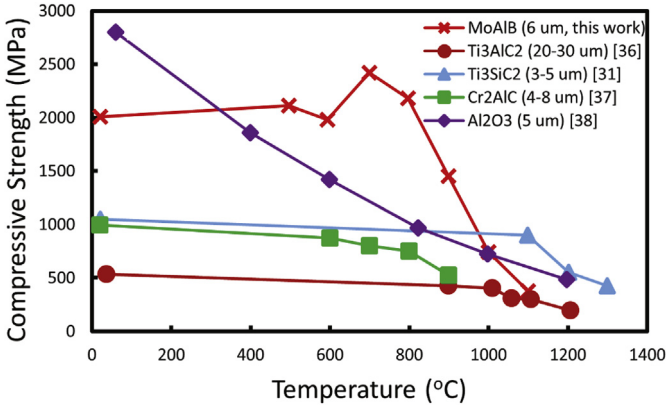

Fig. 8. Temperature dependence of compressive strength of MoAlB compared to typical fine-grained MAX phases and alumina.

below and above BPT temperature can be also traced back to microstructural changes. Although no significant microstructural changes can be observed in samples loaded below the BPT temperature (compare Fig. 6a and b), the microstructures of the samples loaded above the BPT temperature (Fig. 6c–f) show the presence of bent and kinked individual grains, extensive transgranular delamination along basal planes, microcracking and microcrack coalescence. It is reasonable to assume at this juncture that the microcracks, delaminations, etc., are associated with the hysteretic behavior.

Considerable bending and kinking of individual grains has been widely observed in different MAX phases (e.g. Ti_3SiC_2, Ti_2AlC, Ti_3AlC_2, Cr_2AlC, etc. [24–30]). When the strain is recoverable, those deformation processes are responsible for the energy dissipation during cyclic loading observed both below and above their BPT temperatures. However, compared to MAX phases, the occurrence of grain bending and kinking is relatively rare in MoAlB even above the BPT temperature, which renders this mechanism unlikely to be the major cause of the observed energy dissipation and irrecoverable strains observed (Fig. 5) at and above 800 °C. Even after quasi-static compression, cracks are more commonly observed than grain bending in MoAlB loaded above BPT temperatures as illustrated in Fig. 6. Therefore, other microstructural changes, especially transgranular delamination and microcracking, may play important roles in the observed hysteretic behavior.

The kinking model is not the only one used to explain the hysteretic behavior in MAX phases. Instead, Poon et al. [44] used an alternate model, which explained the nonlinear hysteretic behavior of MAX phases by the formation of microcracks and energy dissipation due to friction between crack surfaces during cyclic loading. Although, that model was not successful in completely capturing the macroscopic hysteretic behavior of the MAX phases, in which extensive bending and kinking of individual grains occurs during loading, it might better explain the observed macroscopic stress-strain behavior of MoAlB. In other words, extensive microcracking and delamination above the BPT temperature result in irrecoverable strains and the observed hysteretic behavior in compression, rather than bending and kinking of individual grains that is apparently more difficult in MoAlB.

This difference may be traced to differences in crystal structures and bonding strengths. Although the MAX phases and MoAlB share a similar structure in which Al layer(s) interleave a ceramic sublattice, the crystal structure of the former is hexagonal while that of MoAlB is orthorhombic with strong covalent zig-zag B-B single chains – that are along ⟨001⟩ – within the Mo-B sublattice [45]. The latter results in greater stiffness within the Mo-B blocks when compared to the M-X blocks in the MAX phases. Also, while the C-Al distance in the MAX phases is of the order of 3.8 Å, the Al-B distance at 2.3 Å, is significantly shorter, signifying a much stronger bond in MoAlB. Moreover, the Al–B bonds are even shorter than the B–Mo bonds, within the BM_6 trigonal prisms of the MB blocks, which supports the notion that the bonding between the Mo–B and Al layers is quite strong. At 151 GPa, the shear modulus of MoAlB at RT is significantly higher than those of all 211 Al-containing MAX phases with which they can be compared [9,17]. The shear modulus of MoAlB is closer to that of 312 and 413 Al-containing MAX phases. The fact that the MoAlB structure contains two Al layers, instead of one in the MAX phases, renders it elastic properties even more remarkable and must explain, at least in part, its resistance to deformation. Thus, MoAlB is less prone to kinking and grain bending than the MAX phases which explains the lack of hysteresis at room temperature, and even the relatively small amount of bending and kinking observed above BPT temperature. Above the BPT temperature, although some MoAlB grains are bent, delaminations and microcracks are more dominant, especially within the shear band. The latter can be considered responsible for observed open hysteresis loops in compression.

Recently, it was postulated that ripplocations and not dislocations are responsible for the energy dissipation in layered solids in general and the MAX phases in particular [20]. For ripplocations to nucleate and propagate, sliding and bending of layers is required. However, the strengths of the bonds alluded to above, together with the high elastic properties may be what is preventing the nucleation of ripplocations. Nevertheless, more work is needed to fully understand the origin of the hysteretic stress-stain behavior of MoAlB above its BPT temperature.

Lastly, the fact that UCSs >2 GPa were measured herein, at temperatures up to 800 °C, is noteworthy. These values are even more impressive when the grain size is considered. Typically, at RT, the strengths of ceramics, decrease with increasing grain sizes. A very fruitful avenue of research would be to fabricate MoAlB samples with sub-micron grains and measure their UCS as it is not unreasonable to expect higher UCS. Exceptionally high UCS values reported here are indirect evidence that not only are the grains themselves resistant to deformation, but more importantly, so are the grain boundaries. The fact that MoAlB is readily EDM machinable, forms an alumina layer at higher temperatures when heated in air, and with a moderately low density (6.45 g/cm^3), together with the fact that above 900 °C it can deform significantly and can sustain a large amount of damage before final failure, bodes well for its potential use as a high temperature structural material. Before this can be assessed, it is important to measure its creep properties.

5. Conclusion

The results of uniaxial quasi-static and cyclic compression of MoAlB at temperatures up to 1100 °C show that open stress-strain hysteresis appear above a BPT temperature of 800 °C for this refractory ternary boride. Below the BPT temperature, MoAlB exhibits linear elastic behavior and fails in a brittle manner at stresses exceeding 2 GPa, because the stress is insufficient to cause massive bending, kinking or any other deformation of individual grains. Therefore, this study shows that the mechanical response of MoAlB is quite different than that of the MAX phases wherein fully and spontaneously reversible stress-strain hysteresis loops are typically observed even below the BPT temperatures.

Above the BPT temperature, extensive microcracking has been observed that appears to be predominantly localized in a shear band. Bending and kinking of individual grains, typically observed in the MAX phases, was rare. Once the microcracks form, not surprisingly, the process is irreversible, resulting in small irrecoverable strains in the first loading-unloading cycle. Starting from the second cycle, friction between the microcracked faces and delaminations are proposed to cause the dissipation of energy observed during each cycle, resulting in smaller stress-strain hysteresis loops with increasing number of loading cycles.

Acknowledgments

This work was funded by the National Science Foundation through grants #1729350 and #1729335 awarded to Texas A&M and Drexel Universities, respectively.

References

[1] C. Martini, G. Palombarini, G. Poli, D. Prandstraller, Wear 256 (2004) 608–613.
[2] J. Shappirio, J. Finnegan, R. Lux, D. Fox, J. Kwiatkowski, J. Vac. Sci. Technol. Vac., Surf. Films 3 (1985) 2255–2258.
[3] B.J. Aylett, Br. Polym. J. 18 (1986) 359–363.
[4] E. Sani, L. Mercatelli, M. Meucci, A. Balbo, C. Musa, R. Licheri, R. Orrù, G. Cao, Renew. Energy 91 (2016) 340–346.
[5] J.C. Schlatter, S.T. Oyama, J.E. Metcalfe III, J.M. Lambert Jr., Ind. Eng. Chem. Res. 27 (1988) 1648–1653.
[6] H. Vrubel, X. Hu, Angew. Chem. 124 (2012) 12703–12706.
[7] W.G. Fahrenholtz, G.E. Hilmas, I.G. Talmy, J.A. Zaykoski, J. Am. Ceram. Soc. 90 (2007) 1347–1364.
[8] W. Jeitschko, Monatshefte für Chemie und verwandte Teile anderer Wissenschaften, vol. 97, 1966, pp. 1472–1476.
[9] M.W. Barsoum, MAX Phases: Properties of Machinable Ternary Carbides and Nitrides, John Wiley & Sons, 2013.
[10] S. Kota, M. Agne, E. Zapata-Solvas, O. Dezellus, D. Lopez, B. Gardiola, M. Radovic, M.W. Barsoum, Phys. Rev. B 95 (2017) 144108.
[11] S. Kota, E. Zapata-Solvas, Y. Chen, M. Radovic, W.E. Lee, M.W. Barsoum, J. Electrochem. Soc. 164 (2017) C930–C938.
[12] S. Kota, E. Zapata-Solvas, A. Ly, J. Lu, O. Elkassabany, A. Huon, W.E. Lee, L. Hultman, S.J. May, M.W. Barsoum, Sci. Rep. 6 (2016) 26475.
[13] X. Li, H. Cui, R. Zhang, Sci. Rep. 6 (2016) 39790.
[14] G. Akopov, M.T. Yeung, R.B. Kaner, Adv. Mater. (2017) 1604506.
[15] L. Xu, O. Shi, C. Liu, D. Zhu, S. Grasso, C. Hu, Ceram. Int. 44 (2018) 13396–13401.
[16] M. Radovic, M.W. Barsoum, Am. Ceram. Soc. Bull. 92 (2013) 20–27.
[17] M.W. Barsoum, M. Radovic, Annu. Rev. Mater. Res. 41 (2011) 195–227.
[18] M. Radovic, M.W. Barsoum, A. Ganguly, T. Zhen, P. Finkel, S.R. Kalidindi, E. Lara- Curzio, Acta Mater. 54 (2006) 2757–2767.
[19] J. Griggs, A.C. Lang, J. Gruber, G.J. Tucker, M.L. Taheri, M.W. Barsoum, Acta Mater. 131 (2017) 141–155.
[20] J. Gruber, A.C. Lang, J. Griggs, M.L. Taheri, G.J. Tucker, M.W. Barsoum, Sci. Rep. 6 (2016) 33451.
[21] M.W. Barsoum, T. Zhen, S.R. Kalidindi, M. Radovic, A. Murugaiah, Nat. Mater. 2 (2003) 107–111.
[22] A.G. Zhou, M.W. Barsoum, J. Alloy. Comp. 498 (2010) 62–70.
[23] R. Benitez, W.H. Kan, H. Gao, M. O'Neal, G. Proust, M. Radovic, Acta Mater. 105 (2016) 294–305.
[24] M.W. Barsoum, D. Brodkin, T. El-Raghy, Scripta Mater. 36 (1997) 535–541.
[25] Z.M. Sun, A. Murugaiah, T. Zhen, A. Zhou, M.W. Barsoum, Acta Mater. 53 (2005) 4359–4366.
[26] W. Tian, Z. Sun, H. Hashimoto, Y. Du, J. Mater. Sci. 44 (2009) 102–107.
[27] G.P. Bei, G. Laplanche, V. Gauthier-Brunet, J. Bonneville, S. Dubois, J. Am. Ceram. Soc. 96 (2013) 567–576.
[28] P. Gudlur, A. Muliana, M. Radovic, Compos. B Eng. 58 (2014) 534–543.
[29] L. Hu, R. Benitez, S. Basu, I. Karaman, M. Radovic, Acta Mater. 60 (2012) 6266–6277.
[30] B. Rogelio, H. Gao, M. O'Neal, P. Lovelace, G. Proust, M. Radovic, Acta Mater. 143 (2018) 130–140.
[31] T. El-Raghy, M.W. Barsoum, A. Zavaliangos, S.R. Kalidindi, J. Am. Ceram. Soc. 82 (1999) 2855–2860.
[32] M. Radovic, M.W. Barsoum, T. El-Raghy, S.M. Wiederhorn, W.E. Luecke, Acta Mater. 50 (2002) 1297–1306.
[33] M. Radovic, M.W. Barsoum, T. El-Raghy, J. Seidensticker, S. Wiederhorn, Acta Mater. 48 (2000) 453–459.
[34] M.W. Barsoum, M. Radovic, P. Finkel, T. El-Raghy, Appl. Phys. Lett. 79 (2001) 479–481.
[35] T. Zhen, M.W. Barsoum, S.R. Kalidindi, Acta Mater. 53 (2005) 4163–4171.
[36] N.V. Tzenov, M.W. Barsoum, J. Am. Ceram. Soc. 83 (2000) 825–832.
[37] W. Tian, Z. Sun, H. Hashimoto, Y. Du, J. Mater. Sci. 44 (2009) 102–107.
[38] M. MUNRO, J. Am. Ceram. Soc. 80 (1997) 1919–1928.
[39] M.W. Barsoum, M. Radovic, T. Zhen, P. Finkel, S.R. Kalidindi, Phys. Rev. Lett. 94 (2005) 085501.
[40] A.G. Zhou, M.W. Barsoum, Key Engineering Materials, vol. 434, 2010, pp. 149–153.
[41] A. Murugaiah, M.W. Barsoum, S.R. Kalidindi, T. Zhen, J. Mater. Res. 19 (2004) 1139–1148.
[42] B. Anasori, M.W. Barsoum, MRS Commun. 3 (2013) 245–248.
[43] M. Shamma, V. Presser, B. Clausen, D. Brown, O. Yeheskel, M.W. Barsoum, Scripta Mater. 65 (2011) 573.
[44] B. Poon, L. Ponson, J. Zhao, G. Ravichandran, J. Mech. Phys. Solid. 59 (2011) 2238–2257.
[45] M. Ade, H. Hillebrecht, Inorg. Chem. 54 (2015) 6122–6135.